論文 / 著書情報
Article / Book Information

Title	Experimental investigation of adhesive joint strength and stress-based criteria under tensile/compression-shear stress state using a developed fixture
Authors	Taiga Yamazaki, Keiyu Ikeda, Yu Sekiguchi, Chiaki Sato
Citation	The Journal of Adhesion, Vol. 102, pp. 179-200
Pub. date	2025, 7
Creative Commons	Information is in the article.

THE JOURNAL OF ADHESION
2026, VOL. 102, NO. 3, 179–200
https://doi.org/10.1080/00218464.2025.2528923

Taylor & Francis
Taylor & Francis Group

Experimental investigation of adhesive joint strength and stress-based criteria under tensile/compression–shear stress state using a developed fixture

Taiga Yamazaki[a], Keiyu Ikeda[a], Yu Sekiguchi[b], and Chiaki Sato[b]

[a]Department of Mechanical Engineering, Institute of Science Tokyo, Yokohama, Japan; [b]Laboratory for Future Interdisciplinary Research of Science and Technology (FIRST), Institute of Integrated Research (IIR), Institute of Science Tokyo, Yokohama, Japan

ABSTRACT

A novel test fixture was developed to evaluate the adhesive joint strength under compression-shear stress state with regards to the adhesive layer. The developed fixture enabled high compression – shear strength tests using a tensile testing machine. Tensile, tensile – shear, and shear strength tests were also conducted to compare strength characteristics. The stress – strain relationship showed that the adhesive joints exhibited more ductile behavior as the ratio of compressive stress to shear stress increased. Yield stress and maximum stress values, calculated from the stress – strain diagrams, were plotted on a normal – shear stress plane. Additionally, assuming a plane strain condition for the adhesive joint, the results were plotted on a hydrostatic – equivalent stress plane. The findings demonstrated that adhesive joint strength increased with increasing compressive stress ratio, highlighting the hydrostatic dependency of the strength. Finally, the parameters for the Drucker – Prager yield criterion, Exponential Drucker – Prager yield criterion, and Power law criterion were accurately determined using experimental data from the tensile, tensile-shear, shear, and compression-shear. Applying these results to the strength analysis of adhesive joints is expected to improve the accuracy of crash analysis of automobiles with adhesive joints.

ARTICLE HISTORY
Received 26 March 2025
Accepted 29 June 2025

KEYWORDS
Adhesive joints; Compression–shear; joint strength; mixed mode law; Second-generation acrylic adhesives (SGA); yield criteria

1. Introduction

Adhesive bonding enables the automotive body structures to have high rigidity, dissimilar materials bonding, and high vibration absorption characteristics. Owing to these advantages, the demand for adhesive bonding as a joining method for automotive body structures has increased.[1] Crash safety performance is a critical factor in the automotive industry from the perspective of occupant and pedestrian safety. In the design and development of automobiles, the finite element method (FEM) is widely used alongside crash testing

CONTACT Chiaki Sato csato@pi.titech.ac.jp Institute of Integrated Research (IIR), Institute of Science Tokyo, 4259 Nagatsuta-Cho, Midori-Ku, Yokohama 226-8501, Japan

of the actual vehicle from the viewpoints of financial and time costs.[2] Since the deformation behavior of automobiles during a crash is complex, adhesive joints can be experienced tensile, shear, compression, and combined stress conditions. Therefore, in finite element analysis (FEA), stress-based criteria are applied to represent the deformation and strength of adhesive joints under combined stress conditions.[3–6]

In FEA, adhesive joints are typically modeled using either the continuum mechanics model[3,4,7,8] or the cohesive zone model (CZM).[5,6,9–12] The continuum mechanics model allows for a detailed analysis of mechanical characteristics and is suitable for analyzing the stress distribution and concentration in the thickness direction. However, continuum mechanics models require high computational costs, making them unsuitable for large-scale simulations.[3] Conversely, CZM offers low computational cost, making it suitable for large-scale analyses; however, the CZM cannot analyze the detail of stress distribution in the thickness direction.[3] Additionally, CZM requires fewer input parameters than the continuum mechanics model. Thus, both modeling approaches have advantages and play essential roles in adhesive joint analysis.

In the continuum mechanics model, stress-based criteria are defined using yield criteria, whereas, in CZM, these criteria are defined using mixed mode law. Defining these criteria requires experimentally determined parameters, typically obtained from tensile, tensile – shear, and shear tests.[3,4,12–15] However, the strength of bulk adhesive exhibits hydrostatic pressure dependency.[16,17] Therefore, for accurate parameter determination, experimentally measuring strength under compression – shear stress state in addition to the tensile, shear, and tensile – shear stress state is necessary.

Several studies have investigated the strength of adhesive joints under compression – shear stress. Various methods have been used to test the strength under compression – shear stress. A commonly used approach is the Arcan test, which allows testing under different stress states without requiring changes of the fixture or specimen shape.[18] For example, Créac'hcadec et al.[19,20] Alfonso et al.[21] Suwanpakpraek et al.[22] Cognard et al.[23,24] and Gan et al.[25] measured the compression – shear strength of adhesive joints using an Arcan fixture. While the Arcan fixture can be used for compression – shear testing at the ratio of compressive to shear stress of 1, its structural limitations make it difficult to apply high compressive forces to the specimen. However, adhesive joints in automotive structures might experience combined stress of shear stresses and high compressive stresses.[12] The second method is the compression – torsion test, which requires a specialized torsion-testing machine and cylindrical butt specimens. Ikegami et al.,[26] Isono et al.,[27] and Spaggiari et al.[28] conducted tensile – torsion and compression – torsion tests to measure adhesive joint strength. In this test method, the compression force and torsional torque can

be adjusted to achieve a specific compression-to-shear force ratio. However, even a slight misalignment during bonding can cause the axis of torsion to shift relative to the specimen axis. As a result, the applied torsional moment can introduce an unintended bending moment and additional compressive force, which can generate non-uniform and unstable stress states. Another method involves conducting such tensile and shear tests of adhesive joints in a pressure vessel filled with high-pressure water.[29] Cognard et al. used this method and revealed the hydrostatic pressure dependency of adhesive joint strength. While this method effectively measures hydrostatic pressure dependency, the testing setup has a complex configuration. Moreover, as adhesives can absorb water,[30] their mechanical properties may be affected, potentially influencing strength measurements.[31,32] As discussed above, although several test methods for compression – shear have been proposed, there are still some challenges.

In this study, a compression – shear test method using a developed fixture is proposed. The stress – strain relationship under compression – shear stress is also clarified using the proposed method and the digital image correlation (DIC) method. Furthermore, this study aims to experimentally determine the tensile/compression – shear strength of acrylic adhesive joints and establish parameters for the yield criteria and the mixed mode law in the cohesive zone model. Although crash safety evaluation ultimately requires dynamic and impact testing, a reliable understanding of material behavior under static loading is essential as a foundation. Therefore, this study focuses on static testing as a first step toward future applications. The proposed test method is also designed with future applicability to dynamic conditions. Compared to Arcan specimens, which often involve complex joint geometries that make dynamic loading difficult, the proposed method may be more suitable for high strain rate experiments.

2. Experimental procedure

2.1. Adhesive

A second-generation acrylic adhesive (HARDLOC C-355–20 A/B, Denka Co., Ltd., Tokyo, Japan) was used in this study. The adhesive was cured for 24 h at room temperature (approximately 24 ℃), followed by post-curing at 60 °C for 2 h. Dumbbell-shaped specimens[33] of the cured adhesive (Figure 1(a)) were subjected to tensile testing at a crosshead speed of 1 mm/min. Lateral strain ε_x and longitudinal strain ε_z measurements were performed using the Digital Image Correlation (DIC) method. Image capturing software (VIC-Snap10, Correlated Solutions Inc., Columbia, USA) and image analysis software (VIC-3D9, Correlated Solutions Inc.,

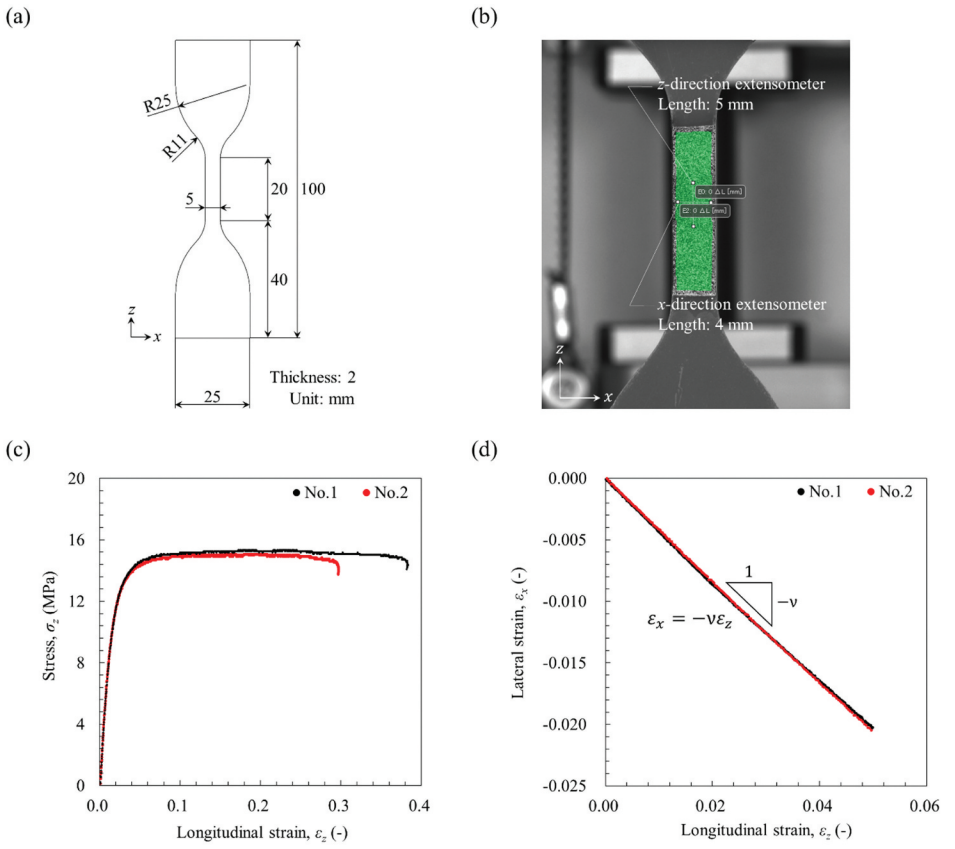

Figure 1. (a) Geometry of JIS K6251–3 dumbbell specimen,[32] (b) setup of extensometers in DIC analysis software, (c) stress – strain diagram, and (d) relationship between lateral strain ε_x and longitudinal strain ε_z.

Columbia, USA) were used (Figure 1(b)). The resulting stress – strain diagram shown in Figure 1(c) indicated elastoplastic behavior with a distinct yielding phenomenon. The Young's modulus E was determined to be 1016 MPa based on the average of two tests, calculated within the strain range of 0.0005 to 0.0025 (Figure 1(a)). The Poisson's ratio ν was determined to be 0.411, based on the average of two tests, calculated as the ratio of ε_x to ε_z (Figure 1(d)).

2.2. Specimens

In the experiment, the strength of the adhesive joints was evaluated for various stress states, including compression – shear. Therefore, the stress angle φ was used to categorize these stress states. As shown in Figure 2, φ is a stress-based phase angle (stress angle) on the $\sigma_z - \tau_{zx}$ plane and is given by Equation (1):

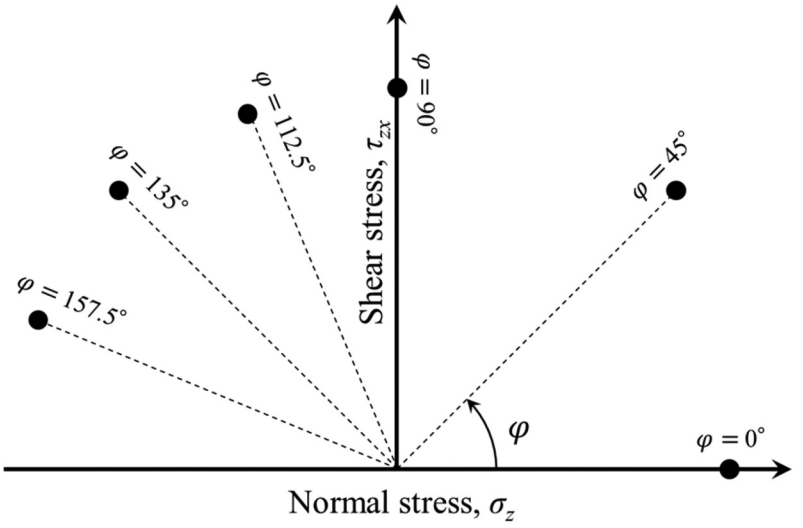

Figure 2. Schematic diagram of stress angle φ in $\sigma_z - \tau_{zx}$ plane.

$$\varphi = \begin{cases} \tan^{-1}\left(\frac{\tau_{zx}}{\sigma_z}\right), & \text{if} \sigma > 0, \\ \tan^{-1}\left(\frac{\tau_{zx}}{\sigma_z}\right) + \pi, & \text{if} \sigma < 0 \text{ and } \tau \geq 0, \\ \tan^{-1}\left(\frac{\tau_{zx}}{\sigma_z}\right) - \pi, & \text{if} \sigma < 0 \text{ and } \tau < 0, \\ +\frac{\pi}{2}, & \text{if} \sigma = 0 \text{ and } \tau > 0, \\ -\frac{\pi}{2}, & \text{if} \sigma = 0 \text{ and } \tau < 0, \\ \textit{Undefined}, & \text{if} \sigma = 0 \text{ and } \tau = 0, \end{cases} \quad (1)$$

where σ_z represents the normal (thickness direction) stress applied to the adhesive joint and τ_{zx} denotes the shear stress. In this study, experiments were conducted at six different φ values: (0°, 45°, 90°, 112.5°, 135°, and 157.5°).

Figure 3 shows the adhesively bonded specimens corresponding to each stress angle, while Table 1 presents the number of samples tested at each stress angle. The compression – shear specimen (Figure 3(a)) was designed with a relatively small bonding area because the compression – shear strength is expected to be higher than the shear strength,[19–29] and reducing the applied load on the test fixture is essential. The tensile, tensile – shear, and shear specimens (Figure 3(b)) were designed based on the specimen geometry used by Horiuchi et al.[4] The bonding surface of the tensile specimen is cylindrical, whereas the other specimens have a rectangular bonding area. In this study, we assumed that the effect of stress concentrations is relatively small due to the large mismatch in Young's modulus between the adhesive and the adherends. In addition, Rune et al.[34] showed through numerical analysis that although stress distribution exists in the elastic region, the distribution tends to stabilize once damage initiates and remains nearly constant during the damage

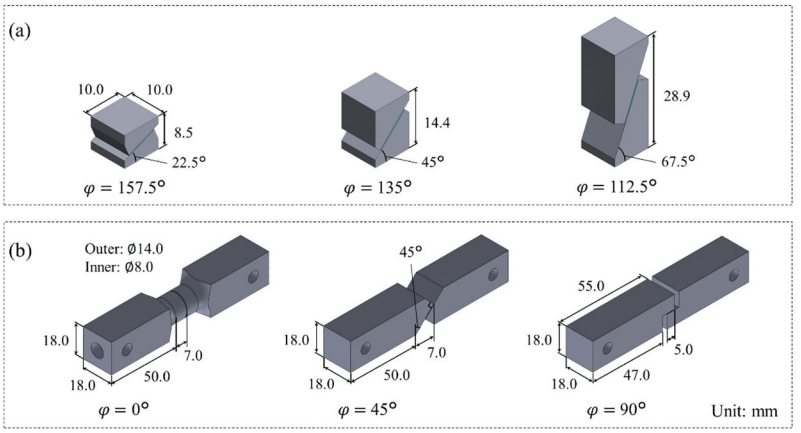

Figure 3. Geometry of adhesive joint specimens for each stress angle φ. (a) compression – shear (φ ($\varphi = 0^{\circ}$), tensile – shear ($\varphi = 45^{\circ}$), and shear ($\varphi = 90^{\circ}$).

Table 1. Number of samples for each stress angle φ.

Stress state	Stress angle φ (°)	Number of samples
tensile	0	3
Tensile-shear	45	3
shear	90	3
Compression – shear	112.5	5
	135	5
	157.5	5

propagation phase. To account for stress concentrations, "beak" have been applied to the adherend in previous studies.[19,20,23,24,29,35,36]

S50C carbon steel was used as the adherend material. To ensure uniformity of the bonded surface and removal of stains, the substrates were sandblasted with #120 alumina powder at an air pressure of approximately 0.6 MPa and subsequently cleaned thoroughly with acetone. The curing conditions of the adhesives were identical to those of the dumbbell specimens. The target adhesive thickness for all specimens was 0.3 mm. Glass beads with a diameter of 0.3 mm were used to control the adhesive thickness of the tensile and tensile – shear specimens. However, in compression – shear tests, the adhesive layer is expected to undergo deformation in the thickness direction due to compressive stress. Therefore, beads may inhibit the deformation of the adhesive layer, making it impossible to accurately evaluate its strength. Thus, a special jig (Figure 4) was designed to control the adhesive thickness without using glass beads.

2.3. Compression – shear test fixture

Figure 5 shows a 3D CAD model of the developed fixture for compression – shear tests. This fixture was designed with reference to the Modified TAST

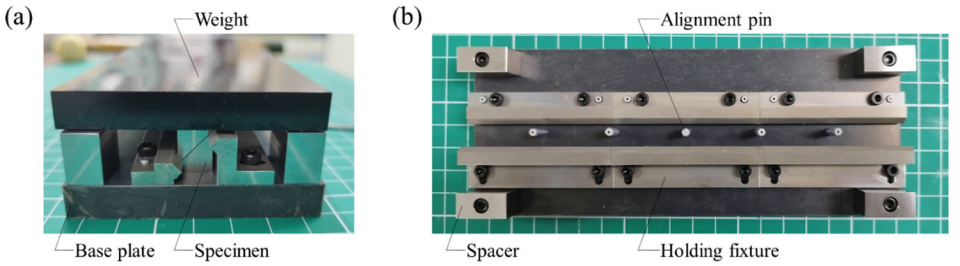

Figure 4. Photographs of a special jig for specimen fabrication: (a) side and (b) top views.

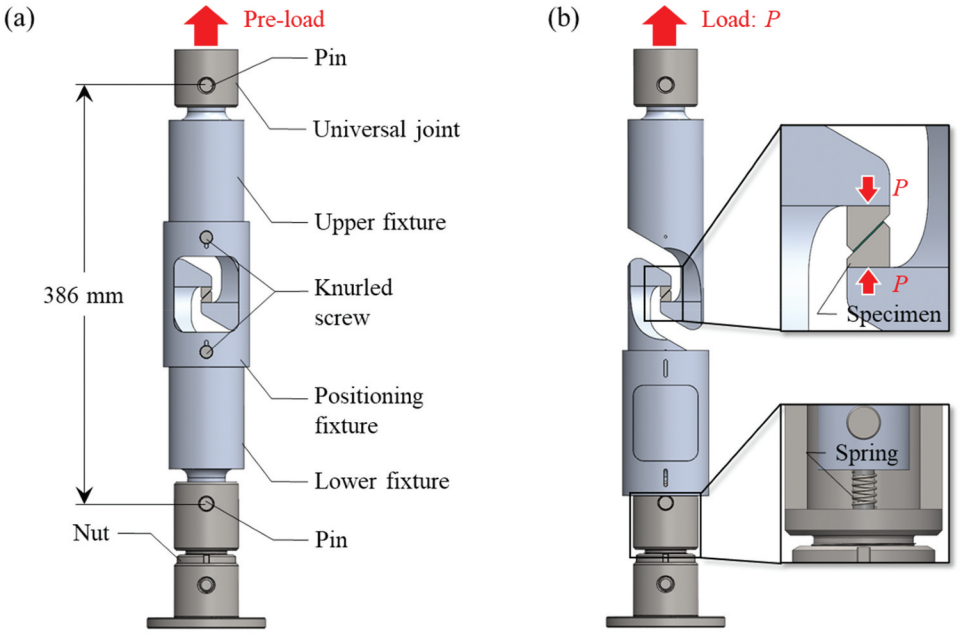

Figure 5. 3D-CAD model of the fixture for compression – shear strength test in adhesive joints: (a) positioning and (b) test configurations.

fixture proposed by Cognard et al.[35,36] developed for measuring the shear strength of adhesive joints. In contrast to the Modified TAST fixture, the developed fixture makes it possible to apply compressive load to the specimen and compression – shear stress to the adhesive layer in the specimen. The compression – shear test fixture consists of three parts: an upper fixture, a lower fixture, and a positioning fixture. The upper fixture is connected to the universal joint, which is attached to the crosshead of the tensile testing machine (Figure 5(a)). The lower fixture, identical in shape to the upper fixture, is similarly connected to the lower part of the tensile testing machine with a pin. Additionally, a spring is installed to prevent the load fluctuation depending on the small gap between the pin and the hole at the start of testing

(Figure 5(b)). It should be noted that spring does not affect the force applied to the specimen. The upward force applied by the spring on the lower fixture is balanced by the downward force transmitted through the lower pin. Therefore, no spring force is transmitted to the specimen. The positioning fixture is fixed, as shown in Figure 5(a), before the beginning of the test, and preliminary loading is performed to ensure accurate alignment of the upper and lower fixtures and prevent the occurrence of moments due to misalignment. The positioning fixture is removed during the test, as shown in Figure 5(b).

The fixture and the specimen are not mechanically fastened but are in contact and can be separated. During testing, the specimen remains in place due to sufficient frictional force between the specimen and the fixture surfaces, and no slipping was observed.

During the test, the adherend moves vertically and horizontally due to the deformation of the adhesive layer. The upper and lower fixtures are designed to rotate around the connection point using pins to accommodate the movement of the adherend. Assuming negligible friction at these pin connections, only a compressive force is applied to the specimen, which ensures that the compressive and shear forces applied to the adhesive joint can be determined from the load of the load cell of the tensile testing machine by resolving the forces based on the inclination of the adhesive layer.

2.4. Stress analysis

Using the newly developed fixture and specimen for compression – shear testing makes it possible to calculate the stress applied to the adhesive layer in the same manner as in a tensile – shear test. Figure 6(a) shows that a Cartesian coordinate system is defined along the adhesive layer. The normal stress σ_z and shear stress τ_{zx} applied to the adhesive layer

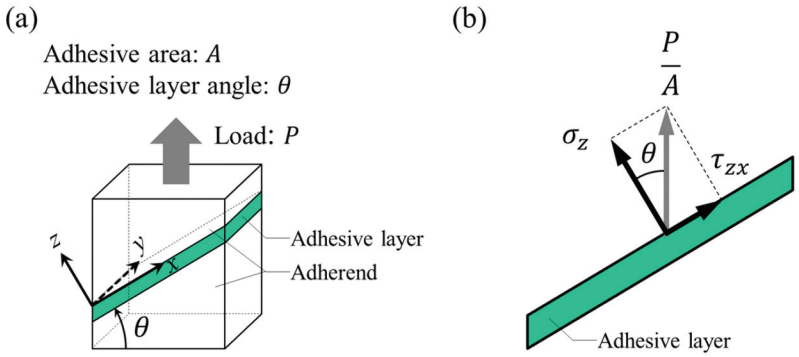

Figure 6. Schematic illustrations of (a) coordinate system and (b) applied stress to the adhesive layer.

(Figure 6(b)) can be obtained using Equations (2) and (3) with the axial load P applied to the specimen and the geometric angle θ between the adhesive layer and a line perpendicular to the direction of load P defined in Figure 6:

$$\sigma_z = \frac{P\cos\theta}{A}, \tag{2}$$

$$\tau_{zx} = \left|\frac{P\sin\theta}{A}\right|. \tag{3}$$

The positive direction of P is shown in Figure 6(a). The sign of the shear stress was ignored, and absolute values were used for evaluation.

The adhesive layer is submitted to a multiaxial stress state by constrained from the adherends. The equivalent von Mises stressσ_{eq} is used to express the yield stress of a material in a multiaxial stress state. In addition, for materials such as adhesives, whose strength depends on hydrostatic pressure, hydrostatic stress σ_{m} is used to represent the stress at a yield on the σ_{eq}–σ_{m} plane.[24,29] σ_{eq} and σ_{m} are expressed by the normal and shear stress σ_i and τ_{ij} $(i,j = x,y,z)$ in the Cartesian coordinate system, as in Equations (4) and (5):

$$\sigma_{\mathrm{eq}} = \sqrt{\frac{1}{2}\left\{\left(\sigma_x-\sigma_y\right)^2+\left(\sigma_y-\sigma_z\right)^2+\left(\sigma_z-\sigma_x\right)^2+6\left({\tau_{xy}}^2+{\tau_{yz}}^2+{\tau_{zy}}^2\right)\right\}}, \tag{4}$$

$$\sigma_{\mathrm{m}} = \frac{1}{3}\left(\sigma_x+\sigma_y+\sigma_z\right). \tag{5}$$

However, determining these stress components from this test is difficult. Therefore, σ_{eq} and σ_{m} were obtained by assuming that the stress state of the adhesive layer is a plane strain state, as the bonded area of the specimen is sufficiently large for the adhesive thickness. In this case, each normal strain and each shear strain are $\varepsilon_x = \varepsilon_y = \gamma_{xy} = \gamma_{yz} = 0$. From the generalized Hooke's law, each stress is obtained as follows:

$$\sigma_x = \sigma_y = \frac{\nu}{(1-\nu)}\sigma_z, \tag{6}$$

$$\tau_{xy} = \tau_{yz} = 0. \tag{7}$$

Using the above Equations, σ_{eq} and σ_{m} in the plane strain state can be calculated using Equations (8) and (9):

$$\sigma_{\mathrm{eq}} = \sqrt{\left(\frac{1-2\nu}{1-\nu}\right)^2{\sigma_z}^2+3{\tau_{zx}}^2}, \tag{8}$$

$$\sigma_{\mathrm{m}} = \frac{1+\nu}{3(1-\nu)}\sigma_z. \tag{9}$$

2.5. Determination of yield criteria and mixed mode law parameters

In this study, the parameters of the Drucker – Prager (DP) and the Exponential Drucker – Prager (EDP) yield criteria were obtained, considering this hydrostatic pressure dependence. The DP yield criterion[37] is expressed in Equation (10):

$$\sqrt{J_2} + \alpha I_1 = k, \tag{10}$$

where α and k are positive material parameters. J_2 is the second invariant of deviatoric stress and I_1 is the first invariant of stress, expressed in Equations (11) and (12):

$$J_2 = \frac{1}{6}\left\{\left(\sigma_x - \sigma_y\right)^2 + \left(\sigma_y - \sigma_z\right)^2 + \left(\sigma_z - \sigma_x\right)^2 + 6\left({\tau_{xy}}^2 + {\tau_{yz}}^2 + {\tau_{zy}}^2\right)\right\}, \tag{11}$$

$$I_1 = \sigma_x + \sigma_y + \sigma_z. \tag{12}$$

In this study, Equation (10) is rewritten in terms of equivalent stress σ_{eq} and hydrostatic stress σ_{m}. The relationships between σ_{eq} and $\sqrt{J_2}$ and between σ_{m} and I_1 are expressed in Equations (13) and (14):

$$\sigma_{\mathrm{eq}} = \sqrt{3J_2}, \tag{13}$$

$$\sigma_{\mathrm{m}} = \frac{I_1}{3}. \tag{14}$$

Additionally, two material parameters α' and k' are defined by Equations (15) and (16):

$$\alpha' = 3\sqrt{3}\alpha, \tag{15}$$

$$k' = \sqrt{3}k. \tag{16}$$

Using Equations (13)–(16), Equation (10) can be rewritten as:

$$\sigma_{\mathrm{eq}} + \alpha'\sigma_{\mathrm{m}} = k'. \tag{17}$$

Therefore, k' is $\sqrt{3}$ times the yield stress in shear. Furthermore, when $\alpha' = 0$, Equation (10) is consistent with the von Mises yield criterion. In contrast, the EDP yield criterion[38] is expressed by Equation (18):

$$a{\sigma_{\mathrm{eq}}}^b + \sigma_{\mathrm{m}} = \sigma_{\mathrm{t}}. \tag{18}$$

where a and b are positive material constants. σ_t is a hardening parameter representing the hydrostatic yield tensile strength of the material.

In the CZM, the stress-based mixed mode law is used to describe mechanical response under combined loading conditions. Instead of using the Cauchy stress tensor, this law is expressed in terms of normal stress σ_z and shear stress τ_{zx} associated with crack propagation in Modes I and II. In this study, the DP yield criterion, EDP yield criterion, and power law (PWL) criterion were used as mixed mode laws. To consider the DP yield criteria and EDP yield criteria as mixed mode laws, they are expressed using σ_z and τ_{zx} as follows:

$$\sqrt{{\sigma_z}^2 + 3{\tau_{zx}}^2} + \frac{\alpha'\sigma_z}{3} = k', \tag{19}$$

$$a\left(\sqrt{{\sigma_z}^2 + 3{\tau_{zx}}^2}\right)^b + \frac{\sigma_z}{3} = \sigma_t. \tag{20}$$

In CZM, only the tractions (normal and shear) and their corresponding separations at the interface are considered. Through-thickness (y direction) strains are not defined, and the formulation is localized to the fracture process zone. For this reason, the cohesive laws in Equation (19) and (20) are written using only the normal (z) and shear (zx) components relative to the interface. The PWL criterion is expressed using positive material parameters A, B, and β as follows:

$$\frac{\sigma_z}{A} + \left(\frac{\tau_{zx}}{B}\right)^\beta = 1. \tag{21}$$

Parameter determination for each yield criterion and mixed mode law was performed by least-squares fitting to the experimentally obtained yield or maximum stress.

2.6. Experimental setup

Figure 7 shows the photographs of the experimental setup (Figure 7(a)), the test fixture for compression – shear (Figure 7(b)), and the test fixture for tensile, tensile – shear, and shear (Figure 7(c)). Strength tests of the adhesively bonded joints were conducted using a tensile testing machine (Autograph AGX-V 50 kN, Shimadzu Co., Ltd., Kyoto, Japan) at a crosshead speed of 0.01 mm/s for quasi-static testing. The applied stresses were determined using loads obtained from the load cell of the testing machine. As the adhesive layer is simultaneously deformed in normal and shear, determining the strain in the normal and shear directions of the adhesive layer was necessary. Therefore, displacement measurements were performed using the DIC method. The same image capturing and image analysis software was used for the dumbbell tensile test.

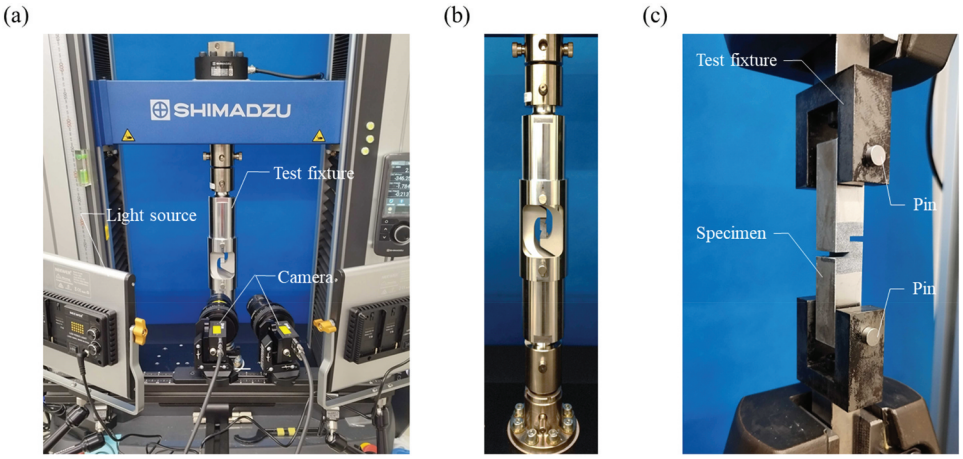

Figure 7. Photographs of (a) experimental setup, (b) test fixture for compression – shear, and (c) test fixture for tensile, tensile – shear, and shear.

As shown in Figure 8, the relative displacement between two adherends was calculated by eliminating the rigid body displacement (red points) of one adherend and setting three measurement points (blue points) on the other adherend in the image analysis software. The displacement at the red points will always be zero, and the red points are reference points of a measured displacement. Therefore, the displacement value obtained at the measurement points indicated by the blue points in Figure 8 are the relative displacement with respect to the red points. Since the blue points and the red points are placed on different adherends, the displacement measured at the blue points is the relative displacement between the adherends. In this study, the relative displacement obtained at three measurement points (blue color) was averaged and used as the displacement of the adhesive layer, assuming that the deformation of the adherend was negligibly small. Furthermore, the strain of the adhesive layer was calculated by dividing this displacement by the adhesive thickness. However, in order to measure the displacement and strain of the adhesive layer more accurately, it is necessary to consider the error caused by the deformation of the adherend. This is a topic for future study.

3. Results and discussion

3.1. Stress – strain diagrams

The stress – strain diagram of the adhesive joints is presented in Figure 9. In this stress – strain diagram, based on the coordinate system in Figure 6, the vertical axis is the nominal stress calculated by equations (2) and (3), and the horizontal axis is the strain calculated by the DIC method. The shear stress – strain diagram (Figure 9(a)) shows elastoplastic behavior with a yielding

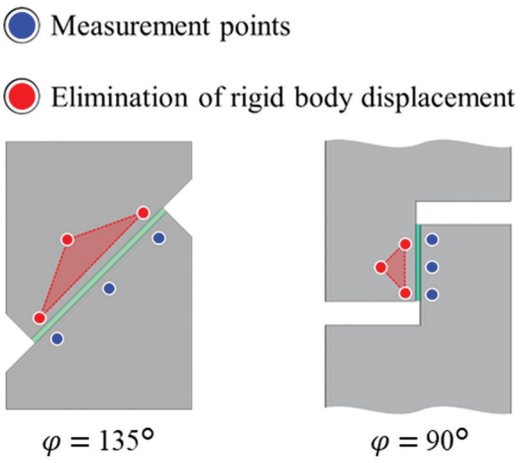

Figure 8. Schematic illustration of measurement points and elimination of rigid body displacement in the DIC method for measuring displacement.

phenomenon, similar to the stress – strain diagram obtained from the dumbbell tensile test of the cured adhesive (Figure 1(c)). The yield shear stress increased with an increase in the stress angle φ, i.e., the ratio of compressive stress to shear stress. A similar trend was observed for the maximum shear stress and failure strain. These findings suggested that the strength of the adhesively bonded joints using acrylic adhesives is dependent on hydrostatic pressure. Moreover, the fracture strain under compression – shear stress ($\varphi \geq 112.5°$) was larger than that under shear stress ($\varphi = 90°$), implying that the energy required for fracture was also larger.

Figures 9(b,c) show the normal stress – strain diagrams. Figure 9(b) presents the results for stress angles of $\varphi = 0°$ and 45°, demonstrating elastoplastic behavior similar to that of the dumbbell tensile test. However, under compression – shear stress in Figure 9(c), the strain shifted toward the tensile side after yielding, despite the application of compressive force. Moreover, the failure strain progressively shifted toward the compressive side as φ increased. The adhesive used in this study has a sea – island structure consisting of two phases: acrylic and elastomer.[39,40] A previous study has reported that cavitation occurs in the elastomer phase, while microcracks develop in the acrylic phase as deformation progresses.[40] Therefore, the observed tensile strain in Figure 9(c) may be attributed to volume expansion caused by cavitation and microcracks despite the application of compressive stress. Furthermore, the causes of the decrease in the tensile strain with increasing φ are discussed, as shown in Figure 9(c). Under compression – shear conditions, the adhesive layer is likely subjected to a triaxial compression stress state, making it likely that the volume expansion due to cavitation and microcracks was suppressed

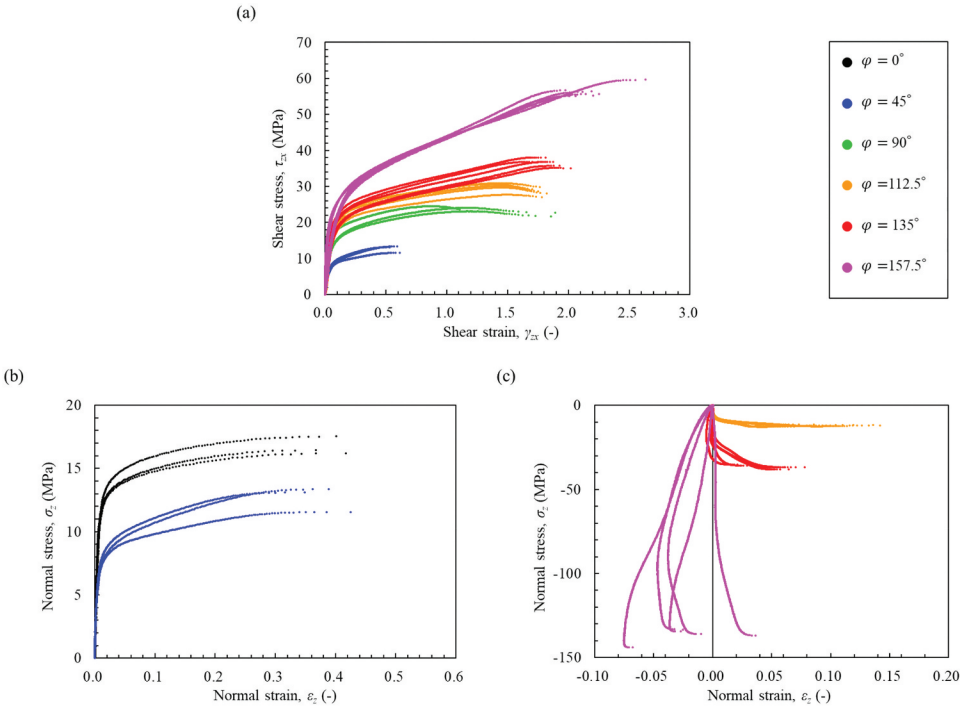

Figure 9. Stress – strain diagram of shear and normal directions: (a) all stress angle φ in the shear direction, (b) φ =0° and 45° in the normal direction, and (c) φ =112.5°, 135°, and 157.5° in the normal direction.

by the higher compression state for larger φ. However, a more detailed investigation of these phenomena is required in the future.

3.2. *Fracture surfaces*

Photographs of the fracture surfaces of the specimens at each stress angle φ are presented in Figure 10. The failure mode was a cohesive failure for all specimens. Additionally, a more detailed observation of the fracture surfaces revealed variations depending on φ. Under tensile shear conditions (φ =45°), linear cracks were observed. Linear cracks are considered to be specific to the combined tensile and shear stress conditions. In the shear condition (φ =90°), no clear cracks were observed, but scale-like fracture surfaces were observed where the adhesive was stretched in the shear direction. Under the compression – shear condition (φ =112.5°, 135°, and 157.5°), fish scale like fracture surface appeared to be stretched in the shear direction for larger φ. This is consistent with the fact that the shear strain at rupture increased with increasing φ (Figure 9(a)).

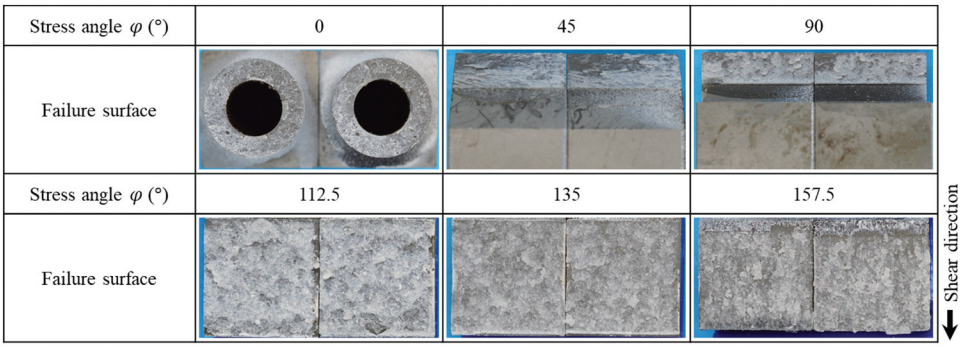

Figure 10. Photographs of fracture surfaces at each stress angle.

3.3. Yield and maximum stress

The yield stress and maximum stress were calculated from the stress – strain diagram (Figure 9). Figure 11 shows a schematic diagram of the stress calculation method. A linear approximation was applied in the elastic region before yielding and in the plastic region after yielding. The intersection of the two lines was identified as the yield stress, while the maximum stress was taken as the maximum stress value in the stress – strain diagram. For tensile – shear, shear, and compression – shear ($\varphi =$ 45°, 90°, 112.5°, 135°, and 157.5°) conditions, yield stress and maximum stress were calculated from shear stress – strain diagrams. For other conditions ($\varphi = 0°$), the yield stress and maximum stress were calculated from the normal stress – strain diagrams.

Figure 12 presents the yield stress and maximum stress for each stress angle. In the $\sigma_z - \tau_{zx}$ plane in Figure 12(a), a significant difference in shear strength was observed between the tensile ($\sigma_z > 0$) and compressive ($\sigma_z < 0$) regions, indicating that the yield and maximum shear stresses increase under higher compressive stress. Additionally, the difference between yield stress and maximum stress widened as φ increased. This trend is attributed to the increase in failure strain and deformation resistance due to high compressive stress. Figure 12(b) shows the yield stress plotted on the σ_{eq}–σ_m plane. Since σ_m and σ_{eq} were calculated using the generalized Hooke's law, the maximum stress after yielding may not be accurate. Therefore, the maximum stress was excluded. Similar to Figure 12(a), the yield stress exhibited an increasing trend with φ, clarifying the hydrostatic pressure dependence of the adhesive joint strength. Furthermore, the variability in compression – shear strength was comparable to that observed under tensile conditions, demonstrating that the developed compression – shear test fixture provides a reproducible experimental result.

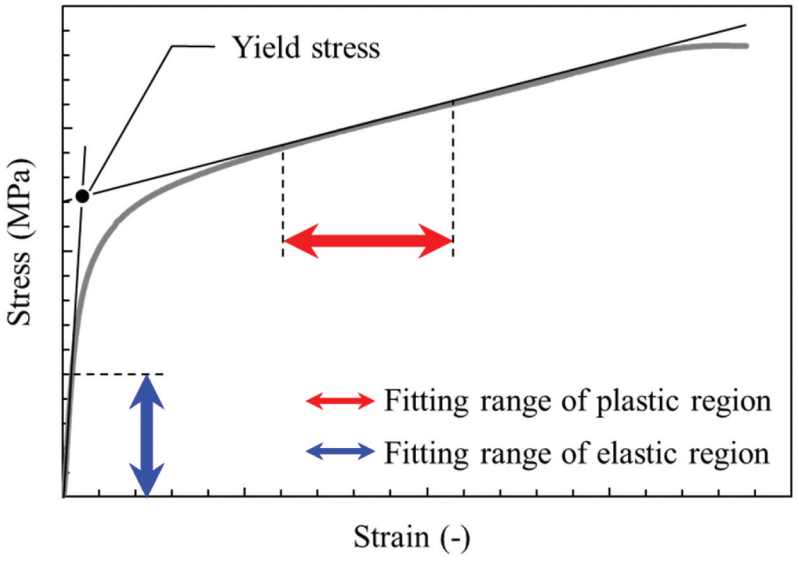

Figure 11. Schematic diagram of yield stress calculation method.

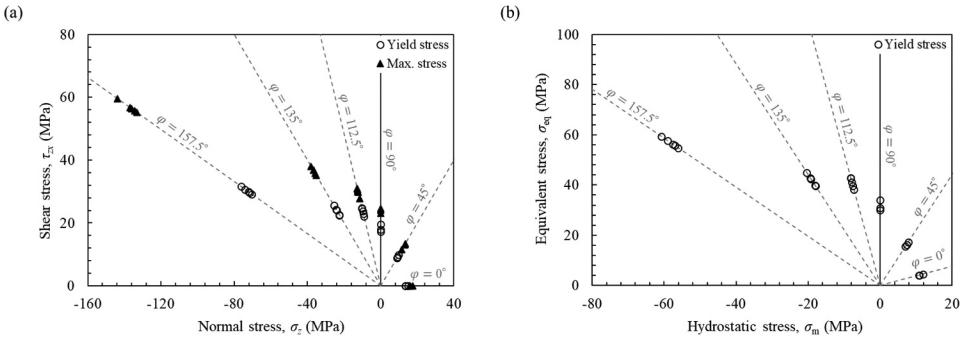

Figure 12. (a) Experimental yield and maximum stress in $\sigma_z - \tau_{zx}$ plane and (b) experimental yield stress in$\sigma_m - \sigma_{eq}$plane.

3.4. Parameters of yield criteria

Figure 13(a) presents the yield surfaces obtained by fitting to the experimental yield stress data (Figure 12(b)). The parameters determined from this fitting (Figure 13(a)) and the coefficient of determination (R^2) are shown in Table 2. The DP yield criterion deviates marginally from the experimental yield stress in shear and compression – shear for $\sigma_m \leq 0$. However, the deviation is significant in tension, where the yield stress is overestimated. Consequently, the coefficient of determination for the DP yield criterion is $R^2 = 0.763$, indicating that it does not adequately capture the yielding behavior of adhesive joints. Conversely, the EDP yield criterion achieves a higher coefficient of determination ($R^2 = 0.945$), showing that it can represent the yielding

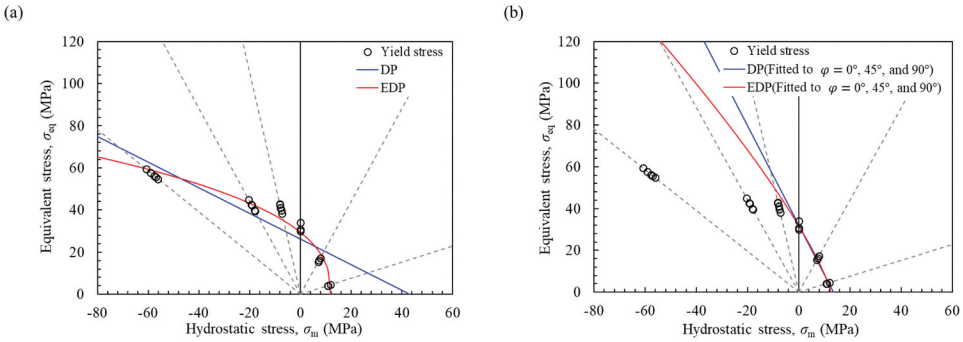

Figure 13. Yield surfaces of DP and EDP criteria in plane strain state: (a) fitted to all experimental data and (b) fitted to only φ =0°, 45°, and 90° ($\sigma_m \geq 0$) data.

Table 2. Parameters of yield criteria determined by least squares method in plane strain state (Figure 14(a)).

Yield criteria	Parameters	Values	R^2
DP	α' (-)	0.609	0.763
$\sigma_{eq} + \alpha'\sigma_m = k'$	k' (MPa)	26.245	
EDP	a (-)	1.987E−3	0.945
$a\sigma_{eq}{}^b + \sigma_m = \sigma_t$	b (-)	2.572	
	σ_t (MPa)	11.942	

behavior accurately (Figure 13(a)). The necessity of compression – shear strength testing is also discussed. Figure 13(b) shows the results of fitting each yield criterion only to the experimental data for $\varphi = 0°$, 45°, and 90°. Both the DP and EDP yield criteria showed good agreement with the experimental data used for fitting. However, substantial deviations occur in compression – shear for $\sigma_m < 0$, resulting in an overestimation of the yield stress. This result highlights the necessity of compression – shear strength testing to accurately determine the yield criterion parameters. Nevertheless, the necessity of compression – shear strength testing depends on the specific application. If an adhesive joint is subjected only to tensile, shear, or these combined stress in a given analysis, compression – shear testing may not be required.

3.5. Parameters of mixed mode law

Figure 14 presents the yield and maximum stress surfaces for each mixed mode law obtained by fitting to the experimental yield and maximum stress data (Figure 12(a)). Table 3 shows the parameters obtained and the coefficient of determination R^2, demonstrating good agreement with the experimental values for all DP, EDP, and PWL criteria. However, at higher compression conditions beyond the experimental range, the yield and maximum stress surfaces exhibited variations depending on the function. Therefore, caution should be exercised when using the parameters obtained in this study to analyze stress states

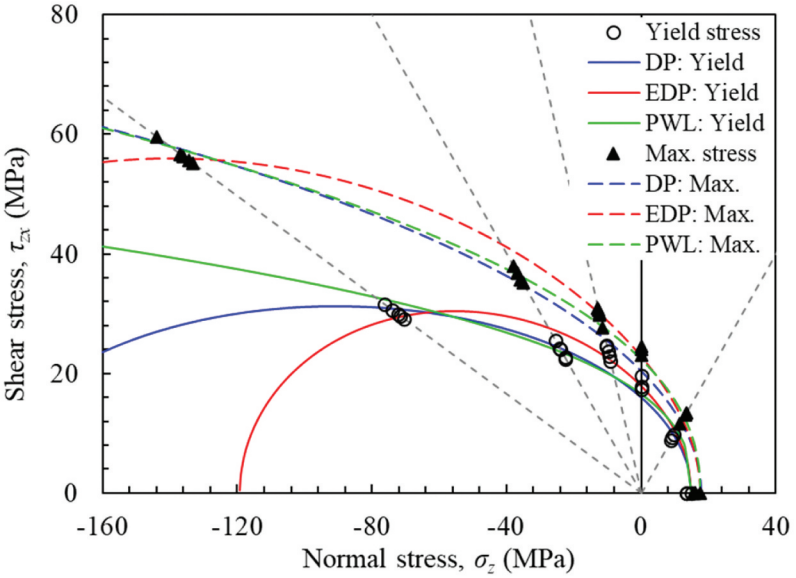

Figure 14. Yield and maximum stress surfaces of mixed mode law for CZM.

Table 3. Parameters of mixed mode law determined by least squares method.

		Yield		Max.	
Mixed mode law	Parameters	Values	R^2	Values	R^2
DP	α' (-)	2.576	0.934	2.934	0.969
$\sqrt{\sigma_z{}^2 + 3\tau_{zx}{}^2} + \frac{\alpha'\sigma_z}{3} = k'$	k' (MPa)	27.456		35.461	
EDP	a (-)	8.260E−2	0.934	9.654E−2	0.975
$a\left(\sqrt{\sigma_z{}^2 + 3\tau_{zx}{}^2}\right)^b + \frac{\sigma_z}{3} = \sigma_t$	b (-)	1.330		1.238	
	σ_t (MPa)	7.988		9.199	
PWL	β (-)	2.700	0.904	2.308	0.977
$\frac{\sigma_z}{A} + \left(\frac{\tau_{zx}}{B}\right)^\beta = 1$	A (MPa)	14.934		17.548	
	B (MPa)	16.601		22.384	

exceeding the experimental conditions. Furthermore, Figure 14 also shows that the maximum stress surface expands in the compressive direction relative to the yield surface, suggesting a significant difference between yield stress and maximum stress under compression – shear stress conditions. When defining the CZM, either the yield stress or the maximum stress criterion is employed as the mixed mode law. However, in analysis involving compression – shear stress states, selecting different stress criteria may lead to substantial discrepancies in the results. Therefore, based on the findings of this study, further investigation is needed into how to define the mixed mode law.

4. Conclusion

This study focused on static testing under multiaxial stress state as a first step of dynamic testing to improve the accuracy of crash analysis of

automobiles with adhesive joints. The compression – shear strength of acrylic adhesives was experimentally determined using the developed compression – shear test fixture. Additionally, tensile, tensile – shear, and shear strengths were performed, and the stress – strain relationships were determined using DIC. Based on these results, the parameters of the yield criterion and the stress-based mixed mode law of CZM were determined. The stress – strain diagrams under compression – shear loading showed more ductile behavior than those under shear loading. The maximum stress and yield stress were also higher than the strength under shear conditions, indicating that the energy required for fracture is higher under compression – shear, suggesting that compression – shear loading may enhance impact resistance. The yield stress and maximum stress calculated from the stress – strain diagrams were plotted in the $\sigma_z - \tau_{zx}$ and $\sigma_{\mathrm{m}} - \sigma_{\mathrm{eq}}$ planes, confirming that the adhesive joint strength exhibits hydrostatic dependence. Finally, the yield criterion and the stress-based mixed mode law were accurately parameterized using the results of compression – shear tests. Applying these results to the strength analysis of adhesive joints is expected to improve the accuracy of crash analysis of automobiles with adhesive joints. However, dynamic testing is essential to accurately capture the behavior of materials and adhesive joints under crash conditions. Therefore, it is desirable to carry out dynamic tests under compression – shear stress to characterize the mechanical properties of adhesive joints in the future.

Author contributions

CRediT: **Taiga Yamazaki:** Conceptualization, Data curation, Investigation, Methodology, Visualization, Writing – original draft, Writing – review & editing; **Keiyu Ikeda:** Investigation, Writing – original draft, Writing – review & editing; **Yu Sekiguchi:** Conceptualization, Methodology, Writing – review & editing; **Chiaki Sato:** Funding acquisition, Supervision, Writing – review & editing.

Disclosure statement

No potential conflict of interest was reported by the author(s).

References

[1] Adams, R. D. *Adhesive Bonding: Science, Technology and Applications*, 2nd ed.; Woodhead Publishing Limited: UK, 2021.

[2] Salanke, S. R. S.; Raju, S. S.; S, T. S.; Srinivas, N. K.; Khot, M. B. A Review on Finite Element Modelling and Experimental Analysis of Crashworthiness Design of Automotive Body. *Int. J. Crashworthiness* 2024, 1–25. DOI: 10.1080/13588265.2024.2418691.

[3] Abe, N.; Sekiguchi, Y.; Sato, C. Parameter Identification of Material Model of Toughened adhesivepolymer for Elasto-Plastic Finite Element Analysis. *J. Adhes. Soc. Jpn.* 2018, *54* (10), 358–366. DOI: 10.11618/adhesion.54.358.

[4] Horiuchi, S.; Sekiguchi, Y.; Ishibashi, Y.; Okamura, M.; Kuroda, I.; Wakamatsu, A.; Tezuka, S.; Tamaki, K.; Iwamoto, M.; Tamaki, H., et al. A Research on Failure Prediction Method for Structural Adhesives with CAE (first Report). In *Proceedings of 2019 JSAE Annual Congress (Spring)* Yokohama, Japan, 2019. <https://tech.jsae.or.jp/paperinfo/ja/content/p201901.325>.

[5] Camanho, P. P.; Davila, C. G. *Mixed Mode Decohesion Finite Elements for the Simulation of Delamination in Composite Materials* 2002. NASA Technical Reports Server (NTRS). <https://ntrs.nasa.gov/citations/20020053651>.

[6] Lee, M.; Yeo, E.; Blacklock, M.; Janardhana, M.; Feih, S.; Wang, C. H. Predicting the Strength of Adhesively Bonded Joints of Variable Thickness Using a Cohesive Element Approach. *Int. J. Adhes. Adhes.* 2015, *58*, 44–52. DOI: 10.1016/j.ijadhadh.2015.01.006.

[7] Takeshi, T. U. Implementation of Elasto Visco-Plastic Constitutive Equations for High Ductile Adhesion into Commercial Finite Element Method. *J. Adhes. Soc. Jpn.* 2018, *54* (11), 429–434. DOI: 10.11618/adhesion.54.429.

[8] Schwarzkopf, G.; Bobbert, M.; Teutenberg, D.; Meschut, G.; Matzenmiller, A. Tolerance Analysis of Adhesive Bonds in Crash Simulation. *Procedia CIRP*. 2016, *43*, 321–326. DOI: 10.1016/j.procir.2016.02.151.

[9] Pinto, A. M. G.; Magalhães, A. G.; Campilho, R. D. S. G.; De Moura, M. F. S. F.; Baptista, A. P. M. single-Lap Joints of Similar and Dissimilar Adherends Bonded with an Acrylic Adhesive. *J. Adhes.* 2009, *85*(6), 351–376. DOI: 10.1080/00218460902880313.

[10] Campilho, R. D. S. G.; Banea, M. D.; Neto, J. A. B. P.; Da Silva, L. F. M. Modelling Adhesive Joints with Cohesive Zone Models: Effect of the Cohesive Law Shape of the Adhesive Layer. *Int. J. Adhes. Adhes.* 2013, *44*, 48–56. DOI: 10.1016/j.ijadhadh.2013.02.006.

[11] Zhang, J.; Wang, J.; Yuan, Z.; Jia, H. Effect of the Cohesive Law Shape on the Modelling of Adhesive Joints Bonded with Brittle and Ductile Adhesives. *Int. J. Adhes. Adhes.* 2018, *85*, 37–43. DOI: 10.1016/j.ijadhadh.2018.05.017.

[12] Ikeda, K.; Orino, K.; Yamazaki, T.; Shimamoto, K.; Sekiguchi, Y.; Sato, C. Three-Point Bending Strength of Double-Hat Beams of High Strength Steel Bonded Adhesively. *The J. Adhes.* 2025, 1–28. DOI: 10.1080/00218464.2025.2465640.

[13] Murakami, S.; Sekiguchi, Y.; Sato, C.; Yokoi, E.; Furusawa, T. Strength of Cylindrical Butt Joints Bonded with Epoxy Adhesives Under Combined Static or High-Rate Loading. *Int. J. Adhes. Adhesive.* 2015, *67*, 86–93. DOI: 10.1016/j.ijadhadh.2015.12.030.

[14] Mu, W.; Xu, Q.; Na, J.; Fan, Y.; Sun, Y.; Liu, Y. Investigating the Failure Behavior of Hygrothermally Aged Adhesively Bonded CFRP-Aluminum Alloy Joints Using Modified Arcan Fixture. *Thin-Walled Struct.* 2022, *182*, 110303. DOI: 10.1016/j.tws.2022.110303.

[15] Beber, V. C.; Baumert, M.; Klapp, O.; Nagel, C. Multiaxial Elastic, Yield and Failure Behaviour of Bonded Joints Using a Hot-Curing Epoxy Film Adhesive: Analytical and Experimental Investigation. *J. Adhes.* 2020, *98*(5), 526–552. DOI: 10.1080/00218464.2020.1850285.

[16] Dolev, G.; Ishai, O. Mechanical Characterization of Adhesive Layer in-Situ and as Bulk Material. *J. Adhes.* 1981, *12*(4), 283–294. DOI: 10.1080/00218468108071207.

[17] Wentingmann, M.; Manousides, N.; Antoniou, A.; Balzani, C. Yield Surface Derivation for a Structural Adhesive Based on Multiaxial Experiments. *Polym. Test.* 2022, *113*, 107648. DOI: 10.1016/j.polymertesting.2022.107648.

[18] Arcan, M.; Hashin, Z.; Voloshin, A. A Method to Produce Uniform Plane-Stress States with Applications to Fiber-Reinforced Materials. *Exp. Mech.* 1978, *18*(4), 141–146. DOI: 10.1007/bf02324146.

[19] Créac'hcadec, R.; Jamin, G.; Cognard, J. Y.; Jousset, P. Experimental Analysis of the Mechanical Behaviour of a Thick Flexible Adhesive Under Tensile/compression-Shear Loads. *Int. J. Adhes. Adhes.* 2013, *48*, 258–267. DOI: 10.1016/j.ijadhadh.2013.09.040.

[20] Créac'hcadec, R.; Sohier, L.; Cellard, C.; Gineste, B. A Stress concentration-Free Bonded Arcan Tensile Compression Shear Test Specimen for the Evaluation of Adhesive Mechanical Response. *Int. J. Adhes. Adhes.* 2015, *61*, 81–92. DOI: 10.1016/j.ijadhadh.2015.05.003.

[21] Alfonso, L.; Badulescu, C.; Carrere, N. Use of the Modified Arcan Fixture to Study the Strength of Bonded Assemblies for Automotive Applications. *Int. J. Adhes. Adhes.* 2017, *80*, 104–114. DOI: 10.1016/j.ijadhadh.2017.09.014.

[22] Suwanpakpraek, K.; Patamaprohm, B.; Phongphinittana, E.; Chaikittiratana, A. Experimental Investigation and Finite Element Modelling of the Influence of Hydrostatic Pressure on Adhesive Joint Failure. *IOP Conf. Ser. Mater. Sci. Eng.* 2020, *886*(1), 012052. DOI: 10.1088/1757-899x/886/1/012052.

[23] Cognard, J.; Davies, P.; Gineste, B.; Sohier, L. Development of an Improved Adhesive Test Method for Composite Assembly Design. *Compos. Sci. Technol.* 2004, *65*(3–4), 359–368. DOI: 10.1016/j.compscitech.2004.09.008.

[24] Cognard, J. Y.; Badulescu, C.; Maurice, J.; Créac'hcadec, R.; Carrère, N.; Vedrine, P. On Modelling the Behaviour of a Ductile Adhesive Under Low Temperatures. *Int. J. Adhes. Adhes.* 2013, *47*, 46–56. DOI: 10.1016/j.ijadhadh.2013.09.024.

[25] Gan, K. W.; Laux, T.; Taher, S. T.; Dulieu-Barton, J. M.; Thomsen, O. T. A Novel Fixture for Determining the Tension/compression-Shear Failure Envelope of Multidirectional Composite Laminates. *Composite Struct.* 2018, *184*, 662–673. DOI: 10.1016/j.compstruct.2017.10.030.

[26] Ikegami, K.; Kajiyama, M.; Kamiko, S.; Shiratori, E. Experimental Studies of the Strength of an Adhesive Joint in a State of Combined Stress. *J. Adhes.* 1979, *10*(1), 25–38. DOI: 10.1080/00218467908544609.

[27] Isono, H.; Yoshimura, J.; Kihara, K.; Sugibayashi, T. Impact Tensile Strength Under the High Temperature of Acrylic Adhesive Using Tubular Butt Joints. *J. Adhes. Soc. Jpn.* 2008, *44*(7), 239–244. DOI: 10.11618/adhesion.44.239.

[28] Spaggiari, A.; Castagnetti, D.; Dragoni, E. A Design Oriented Multiaxial Stress-Based Criterion for the Strength Assessment of Adhesive Layers. *Compos. Part B Eng.* 2018, *157*, 66–75. DOI: 10.1016/j.compositesb.2018.08.085.

[29] Cognard, J. Y.; Créac'hcadec, R.; Da Silva, L. F. M.; Teixeira, F. G.; Davies, P.; Peleau, M. Experimental Analysis of the Influence of Hydrostatic Stress on the Behaviour of an Adhesive Using a Pressure Vessel. *J. Adhes.* 2011, *87*(7–8), 804–825. DOI: 10.1080/00218464.2011.597318.

[30] Han, J.-W.; Sekiguchi, Y.; Shimamoto, K.; Akiyama, H.; Sato, C. Experimental Measurement of Moisture Distribution in the Adhesive Layer Using Near-Infrared Spectroscopy. *J. Appl. Polym. Sci.* 2023, *140*(25), 140(25. DOI: 10.1002/app.53982.

[31] Bowditch. The Durability of Adhesive Joints in the Presence of Water. *Int. J. Adhes. Adhes.* 1996, *16*(2), 73–79. DOI: 10.1016/0143-7496(96)00001-2.

[32] Ramírez, F. M. G.; De Moura, M. F. S. F.; Moreira, R. D. F.; Silva, F. G. A. A Review on the Environmental Degradation Effects on Fatigue Behaviour of Adhesively Bonded Joints. *Fatigue & Fract. Eng. Mater. & Struct.* 2020, *43*(7), 1307–1326. DOI: 10.1111/ffe.13239.

[33] JIS K6251:2017, Rubber, Vulcanized or thermoplastic-Determination of Tensile Stress-Strain Properties. In *JIS Handbook*, Japanese Standards Association; Tokyo Japan, 2018.
[34] Nunes, P.; Marques, E.; Carbas, R.; Akhavan-Safar, A.; Da Silva, L. Quasi-Static and Intermediate Test Speed Validation of SHPB Specimens for the Determination of Mode I, Mode II Fracture Toughness of Structural Epoxy Adhesives. *Eng. Fract. Mech.* 2022, *262*, 108231. DOI: 10.1016/j.engfracmech.2021.108231.
[35] Cognard, J. Y.; Créac'hcadec, R.; Sohier, L.; Davies, P. Analysis of the Nonlinear Behavior of Adhesives in Bonded assemblies—Comparison of TAST and Arcan Tests. *Int. J. Adhes. Adhes.* 2008, *28*(8), 393–404. DOI: 10.1016/j.ijadhadh.2008.04.006.
[36] Cognard, J. Y.; Créac'hcadec, R.; Sohier, L.; Leguillon, D. Influence of Adhesive Thickness on the Behaviour of Bonded Assemblies Under Shear Loadings Using a Modified TAST Fixture. *Int. J. Adhes. Adhes.* 2010, *30*(5), 257–266. DOI: 10.1016/j.ijadhadh.2009.11.003.
[37] Drucker, D. C.; Prager, W. Soil Mechanics and Plastic Analysis or Limit Design. *Q. Appl. Math.* 1952, *10*(2), 157–165. DOI: 10.1090/qam/48291.
[38] Abaqus. *SIMULIA User Assistance 2024*; Dassault Systèmes, 2024.
[39] Hayashi, A.; Sekiguchi, Y.; Sato, C. AFM Observation of Sea-Island Structure Formed by Second Generation Acrylic Adhesive. *J. Adhes.* 2019, *97*(2), 155–171. DOI: 10.1080/00218464.2019.1649148.
[40] Kamiyama, K.; Mikuni, M.; Matsumoto, T.; Matsuda, S.; Kishi, H. Crack Growth Mechanism on SGA Adhesive Joints. *Int. J. Adhes. Adhes.* 2020, *103*, 102690. DOI: 10.1016/j.ijadhadh.2020.102690.